The NCAR Climate System Model, Version One*

BYRON A. BOVILLE AND PETER R. GENT

National Center for Atmospheric Research,[+] Boulder, Colorado

ABSTRACT

The NCAR Climate System Model, version one, is described. The spinup procedure prior to a fully coupled integration is discussed. The fully coupled model has been run for 300 yr with no surface flux corrections in momentum, heat, or freshwater. There is virtually no trend in the surface temperatures over the 300 yr, although there are significant trends in other model fields, especially in the deep ocean. The reasons for the successful integration with no surface temperature trend are discussed.

1. Introduction

Coupled atmosphere and ocean general circulation models (GCMs) are now becoming commonly used for studies of the natural variability of the climate system and its response to changes in forcing. The National Center for Atmospheric Research (NCAR) Climate System Model, version one (CSM-1), is a step toward the development of a comprehensive model of the climate system that is to include chemical and biogeochemical processes in the near future. The initial version is a physical climate model similar to other coupled GCMs. It contains atmospheric and oceanic GCMs, a land surface biophysics and basic soil hydrology model, and a sea-ice dynamics and thermodynamics model. These component models communicate through a driver program called the flux coupler, which controls the time coordination of the integration and calculates most of the fluxes at the interfaces between the model components. No flux corrections in momentum, heat, or freshwater are applied. The modeling system is made freely available to the general scientific community through the World Wide Web (see http://www.cgd.ucar.edu/csm).

The formulation of CSM-1 is summarized in section 2. The spinup procedure prior to fully coupling the CSM is described in section 3. Section 4 contains a brief description of the 300-yr fully coupled integration. Both the successes and deficiencies are briefly described. Section 5 contains the discussion and conclusions. A critique of the spinup procedure is given, and the reasons for the successful integration with no flux corrections and no trend in the surface temperatures are elucidated.

2. Model formulation

CSM-1 is a physical climate model, similar in nature to several other coupled models that have been used for climate studies [see Gates et al. (1996) and Kattenberg et al. (1996) and references therein]. The main new features in the CSM-1 compared to other coupled climate models are the coupling strategy and new state-of-the-art parameterizations, especially in the ocean model. The philosophy has been adopted in the CSM that the most appropriate boundary conditions for the component models are the fluxes at the earth's surface. Those interfacial fluxes that depend directly on the state of more than one component model—for example, turbulent fluxes of latent and sensible heat—are computed within the flux coupler (see Bryan et al. 1996). No flux corrections in momentum, heat, or freshwater are applied. The flux coupler is also responsible for interpolating and averaging between the different grids of the component models while conserving local and integral properties. The surface atmospheric fields are interpolated to the finer grid of the ocean model and the fluxes are calculated on the ocean model grid. The fluxes are then averaged back onto the coarser atmospheric model grid. This becomes increasingly important if the ocean model has much higher resolution than the atmospheric model, because the higher resolution information affects the local turbulent fluxes.

The flux coupler currently allows two separate coupling intervals between itself and the component models. The atmosphere, land, and sea-ice models com-

---

Corresponding author address: Dr. Byron A. Boville, NCAR/CGD, P.O. Box 3000, Boulder, CO 80307-3000.
E-mail: boville@ucar.edu
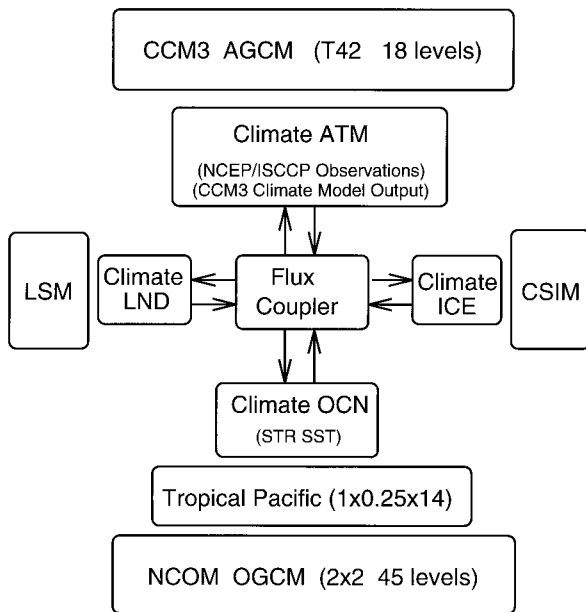
CSM Component Model Configurations

FIG. 1. The CSM-1 component model configurations.

municate at the faster interval, usually 1 h, and the ocean model communicates at the slower interval, usually 1 day. Instantaneous values of state variables and interfacial fluxes time averaged over the coupling interval are passed. Therefore, fluxes are computed from instantaneous state variables and the time integrals of the fluxes applied in the different model components are the same.

The coupling strategy allows component models to be interchanged relatively easily, as illustrated in Fig. 1. Each component model is isolated from the others, and from the coupler, across a predefined message passing interface. Therefore, different models can be used for any component without affecting the rest of the modeling system. For example, the ocean model can be a simple program to supply specified sea surface temperatures, or it can be the full ocean GCM. A tropical Pacific upper-ocean model can also be used for seasonal to interannual simulations. Similarly the atmospheric component can be either CCM3 or a program supplying results of previous simulations or atmospheric analyses. This flexibility is exploited during the spinup phase described below. The execution of the component models can even be distributed across different computers, a feature that has been demonstrated but is rarely used at present.

The atmospheric GCM is CCM3, which is described in Kiehl et al. (1998a), Kiehl et al. (1998b), Hack et al. (1998), Hurrell et al. (1998), and Briegleb and Bromwich (1998a,b) in this issue. CCM3 is the latest generation of the Community Climate Model from NCAR with several major improvements over the previous ver-

sion (CCM2), primarily in the parameterizations of hydrologic processes and in the radiative properties of clouds. CCM3 is a spectral model and the standard configuration, documented in the above papers and used in CSM-1, employs T42 truncation ($\sim$2.9°) with 18 levels in the vertical. Penetrative convection is parameterized by the scheme of Zhang and McFarlane (1995), and Hack's (1994) scheme is used for shallow convection. Cloud fractions and optical properties are computed diagnostically from large-scale variables and convective mass fluxes (Kiehl et al. 1998a). The nonlocal boundary layer turbulent flux parameterization is an updated version of Holtslag and Boville (1993), giving lower boundary layer depths and higher surface humidities. The longwave radiation treats the effects of CO_2, O_3, H_2O, CH_4, N_2O, CFC11, and CFC12. With specified present-day sea surface temperatures (SST), CCM3 produces a globally and annually averaged balance between incoming solar radiation and outgoing longwave radiation to less than 0.5 W m^{-2}.

The ocean GCM is the NCAR CSM Ocean Model (NCOM), described in Gent et al. (1998) and Holland et al. (1998) in this issue. The NCOM configuration for CSM-1 has 2.4° resolution in longitude and variable resolution in latitude, with minimum grid spacing of 1.2° at the equator and in the Arctic and maximum spacing of 2.3° in midlatitudes. In the vertical, 45 levels are used, with 4 equal depth levels in the upper 50 m and 25 levels in the upper kilometer of the ocean. The principal features distinguishing NCOM from the ocean GCMs used in other coupled models are the Gent–McWilliams eddy-mixing parameterization (Gent and McWilliams 1990; Gent et al. 1995), the nonlocal K profile boundary layer parameterization (Large et al. 1994), and the third-order upstream differencing used for heat and salt (Holland et al. 1998). An upper-ocean, tropical Pacific model with higher horizontal resolution is also available on the World Wide Web (http://www.cgd.ucar.edu/csm), which can replace the lower resolution, full depth global ocean model. This ocean model is based on the Gent and Cane (1989) model, but the K profile boundary layer parameterization has been included. This configuration of the CSM is specifically designed for seasonal to interannual variability studies involving the tropical Pacific Ocean.

The land surface biophysics model is LSM 1, described in Bonan (1998) in this issue. In the current configuration of CSM-1, LSM runs on the same grid as CCM3, although this restriction will be relaxed in future versions of the CSM. Rather than attempting to define an average land and vegetation type for each grid cell, LSM subdivides the grid cell into a maximum of four different surfaces, allowing differing vegetation types, bare soil, lakes, and wetlands to be treated separately. The areas of each type within a grid cell are specified and time invariant. Grid cell average fluxes are determined by area averaging the fluxes from each surface type. LSM contains a simple model for the column hy-

drology within each grid cell subdivision and computes both surface and subsurface runoff. However, this runoff is not yet routed back to the oceans through a river runoff model in CSM-1. Instead, CSM-1 contains a simple scheme to maintain the freshwater balance in the ocean and sea-ice models. The precipitation field from CCM3 is multiplied by a time-dependent, but spatially invariant, factor that is the ratio of the globally averaged evaporation to precipitation over oceans and sea ice. This is equivalent to instantaneously distributing the excess water flux from atmosphere to land—that is, the difference between area-integrated evaporation and precipitation—over the ocean and sea ice. This ratio is computed in the flux coupler at every ocean coupling interval of 1 day and is typically about 1.03. This ensures global conservation of freshwater in the CSM-1 when the ocean model is run in synchronous mode (see section 3). A river runoff model is under development and will replace the precipitation scaling scheme in the next version of the CSM.

The precipitation scaling scheme used here is completely different in nature from the flux corrections, or flux adjustments, often included in coupled climate models. Flux corrections are constant additive terms that vary geographically and, usually, seasonally, but that are independent of the coupled model state (see, e.g., Meehl et al. 1997). Flux corrections are typically used to compensate for inconsistencies in the fluxes between components of a coupled model and to ensure that the systematic errors in coupled model simulations remain small. They usually result in a global imbalance between the fluxes coming out of the atmospheric model and the fluxes received by the ocean, sea-ice, and land models. Often the flux corrections have an implied poleward heat transport that is comparable to that in the ocean component. In complete contrast, the precipitation scaling scheme in CSM-1 is present solely to ensure conservation of freshwater in the absence of a river runoff model. Based on short integrations without the precipitation scaling scheme, we believe that it does not greatly affect the simulation. The volume-averaged salinity increases slowly when the precipitation scaling scheme is not operating, but the rate of increase is small compared to the trend in horizontally averaged salinity in the coupled integration. The surface ocean freshens considerably and the deep ocean becomes much more saline (as described below in section 4).

The sea-ice model, described in Weatherly et al. (1998) in this issue, is very similar to the model used in Washington and Meehl (1996) and has been adapted from that model. The ice thermodynamics is based on the three-layer model of Semtner (1976). For ice dynamics, the model employs the cavitating fluid rheology of Flato and Hibler (1990, 1992). During the development of CSM-1, it was found that the iterative solver in the ice dynamics was not converging to the correct solution in regions of compact, thick ice. In such regions, where the ice strength is sufficient to prevent

ice convergence, some residual convergence is often produced in the ice dynamics solution, resulting in continually increasing ice thickness. Regions of erroneous residual convergence can be readily diagnosed, but there is no obvious way to correct the solution. In consequence, a correction step has been added to the ice dynamics, in which the erroneous increase in ice volume is removed uniformly and redistributed to the edge of the converging region [see Weatherly et al. (1998) for details]. This correction does not affect increases in ice depth due to thermodynamic effects in the converging region. An improved sea-ice rheology model is being actively developed for the next generation of the CSM, which will eliminate this convergence problem. We have also found that the roughness length over sea-ice used in CSM-1 (4 cm) is much larger than it should have been. A more typical roughness length of 0.5 mm will be used in future simulations, decreasing the drag coefficients over sea ice by a factor of about 4, since the roughness length enters logarithmically.

There were only two code changes made during the fully coupled CSM-1 simulation described below. The first was made at year 10 and was a minor correction to the freshwater budget between the ocean and sea-ice models that ensured conservation between them. This error was very small, but had been present throughout the integrations to this point. The second code change was made at year 50, when the communication interval between the atmosphere, land, and sea-ice models and the flux coupler was increased from every time step of 20 min to every three time steps, or 1 h. This second change was made for efficiency reasons, because it greatly reduced the amount of information passed between CCM3 and the flux coupler. An overlap run of 10 yr passing information every time step showed that this change did not affect the statistical equilibrium of the coupled simulation.

3. Spinup procedure

To perform relatively drift-free coupled simulations, compatible initial states for the component models are required. To ensure compatibility, several sequential integrations of the component models are needed, and this is referred to as the spinup procedure. The first stage of the spinup procedure is to obtain equilibrated solutions for the atmosphere and ocean GCMs using forcing from observations.

1) The atmospheric model, CCM3, and the land model, LSM1, were integrated for 6.5 yr using the climatological monthly SST dataset from Shea et al. (1990) (STR). Sea-ice extent was also diagnosed from the SST dataset and the consequence of this is described below. Daily data from the last 5 yr of the run were archived for state variables at the lowest model level and for the radiative fluxes at the surface. This equilibrium annual cycle simulation of CCM3
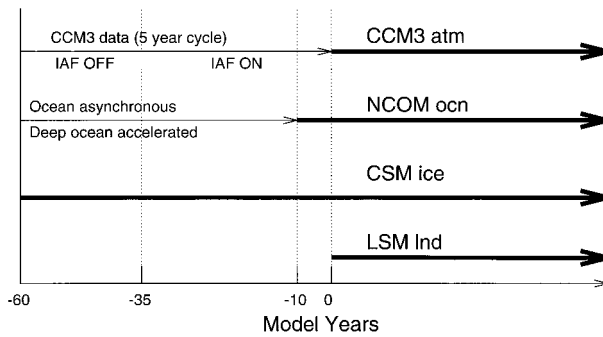
CSM Spin-up Procedure

FIG. 2. The CSM-1 spinup procedure.

is documented in several papers and the land solution is described in Bonan (1998) in this issue.

2) NCOM was integrated to an equilibrium annual cycle solution using bulk forcing. The forcing uses surface insolation from the International Satellite Cloud Climatology Project, reanalyzed atmospheric fields from the National Centers for Environmental Prediction (NCEP), precipitation estimates from the microwave sounding unit, and the freshwater flux has a weak restoring term to the salinity dataset of Levitus (1982). The surface insolation, specific humidity, and precipitation are scaled by constant factors in order to produce global surface energy balance. Sea-ice extent in this integration is also diagnosed from the STR SST dataset. Both the forcing and the solution are described in Gent et al. (1998) in this issue. The equilibrium solution for 1 January is used as the initial condition for the next phase of the spinup and no further use is made of the observational datasets. In particular, the weak restoring to the Levitus dataset in the freshwater flux is *not* included in the subsequent spinup phases or in the fully coupled run.

After obtaining solutions for the atmosphere and ocean with observed forcing, the spinup of the coupled model was carried out as depicted in Fig. 2. The sequence of integrations carried out for the CSM was as follows.

3) The daily values of the required atmospheric data for the last 5 yr of run 1) were used as forcing for an integration of the ocean and sea-ice models. Initial conditions for the ocean were the solution described above in 2) and for the ice was the final state from a previous, short coupled ocean and sea-ice integration. The ocean model was run in accelerated mode, as is commonly done to minimize the computation required to approach equilibrium in the deep ocean (see Bryan 1984; Danabasoglu et al. 1996). The tracer equations were accelerated by a factor of 6 with respect to the momentum equations and the deep

ocean was accelerated by a factor of 10 with respect to the surface. This vertical acceleration factor varies smoothly with depth, and there is no vertical acceleration in the top 25 model levels, which corresponds to the upper kilometer of the ocean. Because of the acceleration, it was appropriate to apply a 14-day running mean to the fluxes driving the ocean. This eliminates the high-frequency component of the forcing, which cannot be realistically modeled when the ocean model is run in accelerated mode. The ice-albedo feedback was turned off, so that net insolation at the surface from CCM3 was used to drive the ocean. Thus, the net insolation reflects the STR ice distribution, not that in the active ice model. The globally integrated freshwater flux at the ocean and sea-ice surface is balanced because the coupler uses the precipitation factor described earlier. However, balancing the freshwater input did not ensure that the total freshwater in the ocean and ice models is constant, because the ocean was run in accelerated mode. Danabasoglu et al. (1996) show that running the ocean in accelerated mode does not conserve the global heat and freshwater in the ocean even though the surface heat and freshwater fluxes are balanced. This integration was run for 25 yr, which was five cycles of the CCM3 data, but the deep ocean tracer fields experience an effective spinup time of 250 yr.

4) The ice-albedo feedback was then turned on by specifying the downward solar radiation at the surface and letting the sea-ice distribution from the model determine the albedo. This integration was run for another 25 yr, so that the deep ocean tracer fields have experienced an effective total spinup of 500 yr.

5) The acceleration was then turned off and the ocean model was run subsequently in synchronous mode. The 14-day running mean was also turned off, so that the ocean and sea-ice received daily fluxes. The daily balancing of precipitation and evaporation remains, and now this ensures that the total freshwater in the ocean and sea-ice models is conserved. This integration was performed for another 10 yr, which allows the momentum and upper-ocean mass fields to adjust correctly to the CCM3 forcing. This cannot be achieved when the ocean tracer equations are accelerated with respect to the momentum equation.

6) Finally, the fully coupled model was integrated for 300 yr. The initial conditions for CCM3 were the 1 January fields taken from the end of run 1, and the land model initial conditions were from the dataset used to initialize the land model in run 1. The balancing of precipitation and evaporation over the active ocean and ice areas remains during this fully coupled run, so that the total freshwater in the CSM-1 is conserved. It should be emphasized again that there is no salinity restoring term in the ocean model during integrations 3–6.

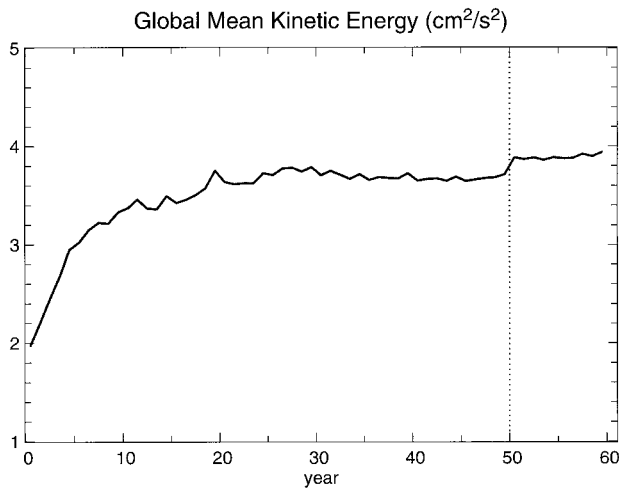The global average kinetic energy in NCOM over the

FIG. 3. Globally averaged kinetic energy from the ocean model during the spinup procedure. The solid line is the 12-month running mean and the shading indicates the annual range of the monthly mean values.
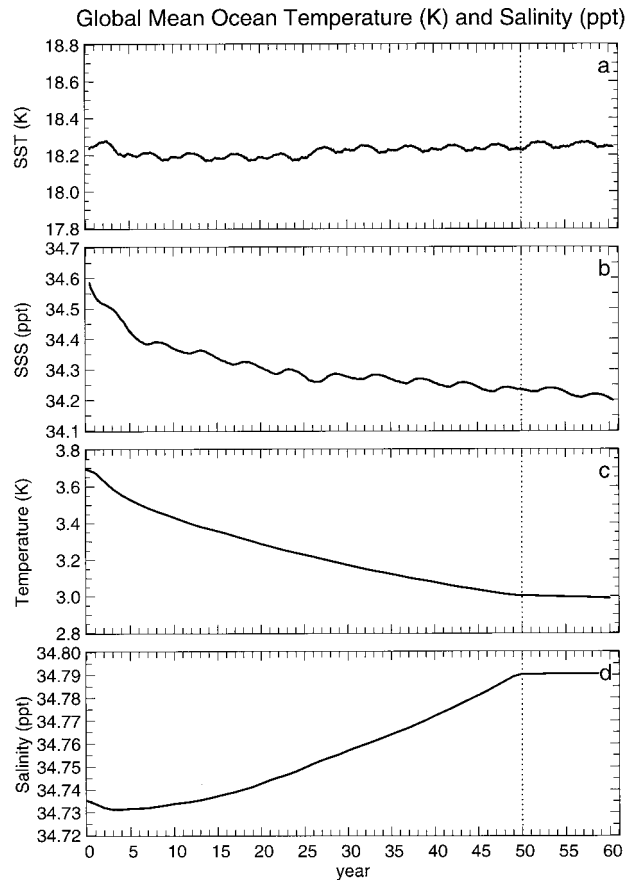

FIG. 4. (a) Average SST, (b) average SSS, (c) globally averaged potential temperature, and (d) globally averaged salinity from the ocean model during the spinup procedure. In (a) and (b) the solid line is the 12-month running mean and the shading indicates the annual range of the monthly mean values.

60-yr spinup integration is shown in Fig. 3. It takes about 25 yr for the ocean to reach an equilibrium value in this quantity, and it is about twice the kinetic energy in the ocean alone integration described in 2) above, which uses monthly mean forcing. The kinetic energy increased another 5% after year 50 because of the daily forcing, as opposed to the 14-day running mean forcing in the first 50 yr.

The area-averaged SST and sea surface salinity (SSS) from the 60-yr spinup are shown in Fig. 4. Both the mean SST and the amplitude of the annual cycle are virtually unchanged during the spinup and have negligible trends. In contrast, however, there is a strong trend in the SSS. The mean SSS starts close to the observed value of 34.6 ppt, decreases rapidly over the first 20 yr, then more slowly over years 20–40. It continues to decrease slowly over years 40–60 so that, at the end of the spinup, the SSS is 34.2 ppt. This is a significant freshening of the upper ocean, which is caused by different freshwater forcing from CCM3 compared to the ocean alone spinup. However, the trend in the SSS is quite small at the end of the spinup procedure.

The volume-averaged ocean potential temperature and salinity from the spinup runs are also shown in Fig. 4. The total heat content of the ocean decreases by about 15% during the first 50 yr of the spinup, which is a significant decrease. The rate of decrease reduces between years 50 and 60 because the ocean model is run in synchronous mode. The volume average salinity also changes significantly over the first 50 yr, and would adjust further if the accelerated spinup was continued. However, the freshwater in the ocean and sea-ice models is conserved after the acceleration is turned off. Thus, the change in the volume average ocean salinity over years 50–60 matches the change in the volume of sea ice, and both are quite small. Figure 5 shows the area-
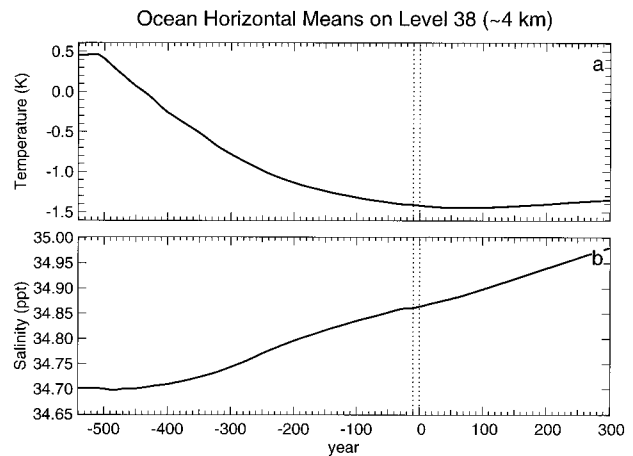

FIG. 5. (a) Area-averaged potential temperature, and (b) area-averaged salinity for level 38 in the ocean model, which is at about 4-km depth. The figure shows both the spinup procedure and the fully coupled run.

Ice Area (10^{13} m^2)
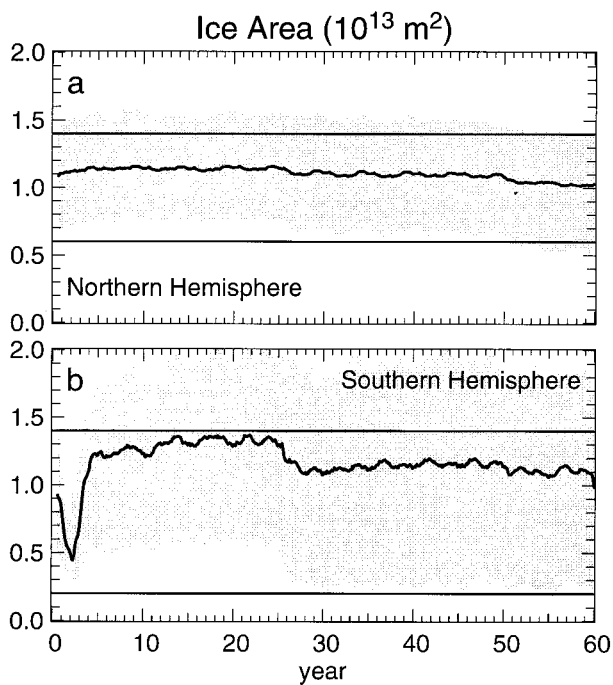

Ice volume (10^{13} m^3)

FIG. 6. (a) Northern Hemisphere ice area, and (b) Southern Hemisphere ice area during the spinup procedure. Solid lines are the 12-month running mean from the model and observational estimates of the maximum and minimum areas. The shading indicates the annual range of the model monthly mean values.

FIG. 7. The same as Fig. 6 but for sea-ice volumes.

averaged potential temperature and salinity at level 38 of the ocean model. This level is at about 4-km depth, and is the uppermost level where the vertical acceleration is a factor of 10 compared to the surface. Hence, the abscissa of Fig. 5 covers 510 yr for the full spinup procedure. The average potential temperature decreases significantly from 0.5°C to −1.4°C during the spinup, but most of the adjustment has ocurred by the end of 500 yr. The average salinity also has a significant trend changing from 34.70 to 34.85 ppt during the spinup, and would adjust further if the spinup phase was continued. This spinup procedure will be discussed and critiqued in section 4.

The sea-ice areas in both hemispheres over the 60-yr spinup are shown in Fig. 6 together with estimates of their observed annual ranges from Gloersen et al. (1992). The annual range of Arctic ice area does not vary much during the spinup procedure and is close to the observations. In the Antarctic, the area of sea ice decreases rapidly at first, but then recovers just as quickly, so that the maximum and minimum values are considerably larger than the observed values. The simulated values reflect the diagnosed ice area from the STR dataset, which is governing the albedo in the first 25 yr. The STR diagnosed area is larger than the observations because the ocean is assumed to be completely ice covered in areas where the SST is −1.8° C. It is not clear that switching the ice-albedo feedback off over the first 25 yr is absolutely necessary. Bryan (1998) in this issue
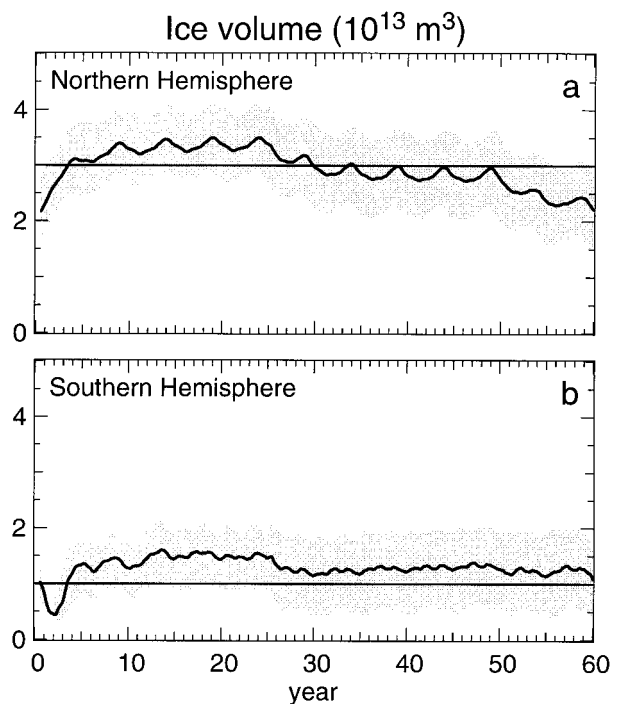
shows a spinup calculation with the ice-albedo feedback on from the start. In this calculation the Southern Hemisphere ice area decreases even more at the start and takes considerably longer to recover toward observed values. Switching the ice-albedo feedback off over the first 25 yr alleviates this problem.

The ice-albedo feedback actually has little effect on the maximum ice area around Antarctica, since it occurs in winter, when there is little or no insolation at the latitudes where sea-ice forms. The atmospheric temperatures at that time, on which the turbulent fluxes are based, are very cold in regions where ice was diagnosed during the CCM3 integration 1. This results in strong cooling from the ocean surface and ice formation until the ice extent closely matches that in the CCM3 integration 1. The ice-albedo feedback has a stronger impact on the minimum ice area, which occurs in summer when the insolation is strong and the low-level atmospheric temperatures are not very cold, even in regions where ice is diagnosed. In consequence, the annual cycle of ice area around Antarctica is too large during the latter part of the spinup.

Like the ice area, the Southern Hemisphere ice volume in Fig. 7 also decreases rapidly at first and recovers quickly to a value considerably greater than the observational estimate. After year 25 it reduces somewhat, but remains a little larger than the observations. The ice volume in the Northern Hemisphere increases over the first 20 yr, and then decreases slowly so that at year 60 it has returned to its initial value. Note that the observed ice volumes are not well known, whereas the ice areas
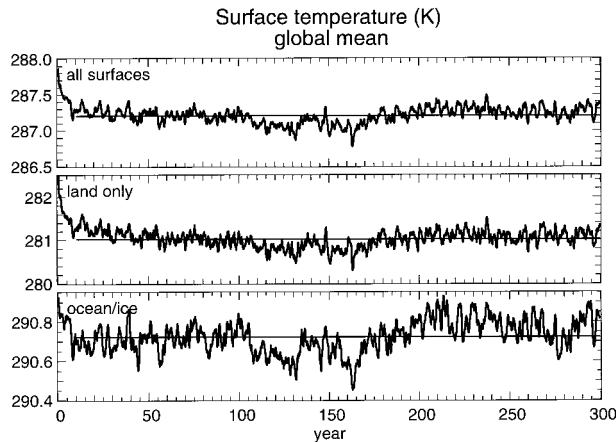
FIG. 8. Twelve-month running means of surface temperature: (a) globally averaged over all surfaces, (b) over land only, and (c) over ocean and sea ice. The mean of each series from years 11 to 300 is indicated by a horizontal line.

are well known from observations. The "observed" volumes have been calculated using estimates of average ice thicknesses of 3 m in the Arctic and 1.25 m in the Antarctic.

4. The coupled simulation

The fully coupled model was integrated for 300 yr. The global annual mean surface temperatures shown in Fig. 8 exhibit an adjustment of about 0.7 K over the first 5–10 yr of the simulation and are remarkably stable afterward. The initial adjustment is largely due to a 1.5 K decrease in the land temperatures, resulting from the fact that a generic initial condition was inadvertently used in LSM1 instead of the equilibrated state from the end of the CCM3/LSM1 simulation 1. There is also a rapid adjustment of the ocean temperatures in the first few months of the simulation, with the initial month being about 0.2 K warmer than any subsequent month. The coupled simulation has strong variability on multiyear timescales, but no surface temperature trends after year 10. The trends in land and ocean/ice temperatures, determined by least squares fits for years 11–299, are 0.03 K century^{-1} and are small compared to the standard deviations of the annual means of 0.2 K and 0.07 K, respectively. A SST trend map is not shown because there are no statistically significant trends in surface temperature, even on a regional basis.

Figure 9 shows the decadal average SST from years 91 to 100 of the coupled model run and the difference between the model and the STR dataset. Figure 9 is essentially indistinguishable from the equivalent figure for any decade (after the first) of the 300-yr simulation, because the interdecadal variability of surface temperature is small. Over much of the globe, the SST errors are less than 1 K, even in the equatorial Pacific, where recent analyses suggest that the STR estimate of cli-

matological SST is 1 K too warm; see Reynolds and Smith (1994). The marine stratus regions off the western coasts of North and South America and off Africa are too warm by 2–3 K, resulting from a bias in cloud simulation in CCM3. In higher northern latitudes, a shift in the Gulf Stream is apparent with a warm bias off Labrador, whereas the SSTs are too cold near Norway and in the North Pacific. These biases are accompanied by shifts in the ice distribution. The high-latitude southern ocean is slightly too warm, although the largest differences with climatology occur in the southern Indian Ocean where very strong gradients are found in both model and observations. The observations of SST are somewhat uncertain in that region, but the deviations of the Antarctic Circumpolar Current around and over the Kerguelan Plateau may be misrepresented in the ocean model.

The interdecadal and subdecadal interannual variability of the surface temperatures are shown in Fig. 10. Saravanan (1998), in this issue, gives a detailed comparison of the SST variability with observations. The quantities shown here include land and sea-ice temperatures in addition to SST. The decadal variability is computed as the standard deviation of the 29 decadal means for years 10–299. Interdecadal variability is very small, except in high latitudes, with the largest signals being associated with changes in sea-ice cover in the North Atlantic and in the Weddell Sea. The North Atlantic variability is also associated with a low-frequency (>70 yr) fluctuation in the overturning circulation, which is discussed in Capotondi and Holland (1998, manuscript submitted to *J. Climate*). Higher-frequency interannual variability, defined as the square root of the difference between total and interdecadal variance, is considerably larger than decadal variability over most of the globe. The variability is particularly large over the Arctic and northern oceans and landmasses, as expected from observations. A somewhat weaker than observed ENSO signal can be seen in the tropical Pacific, although the variability is largest in the western Pacific rather than where it is observed in the Central Pacific [see Meehl and Arblaster (1998) in this issue].

The Northern and Southern Hemisphere ice areas are shown in Fig. 11 together with the last 10 yr of the spinup. The area covered by sea ice in the Northern Hemisphere increases for the first 20 yr of the coupled simulation, then stabilizes with about 15% too much ice area compared to observations. The excess is somewhat larger in winter than in summer. There is an 80-yr period from years 110–190 with increased winter ice areas, then the area returns to its earlier, somewhat overly large value. This increased winter ice is quite thin and does not have a clear signal in the total ice volume (shown in Fig. 12). The Northern Hemisphere ice volume also increases fairly rapidly for the first 20 yr of the coupled simulation, then nearly stabilizes, with a slow increase continuing until about year 160. On average there is about 25% too much total ice volume compared to the
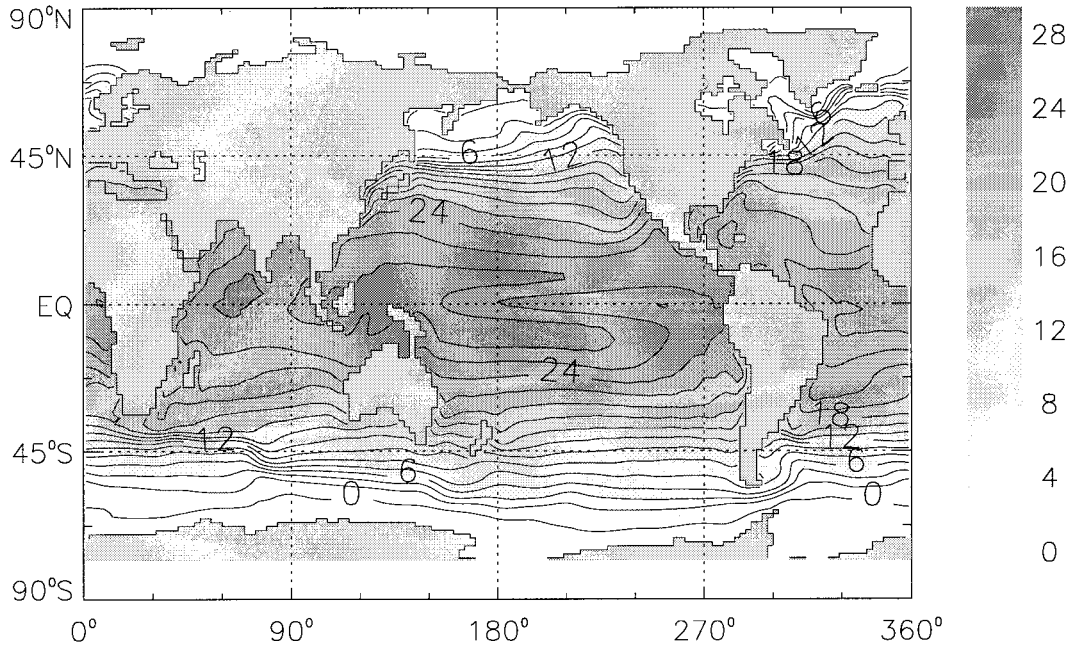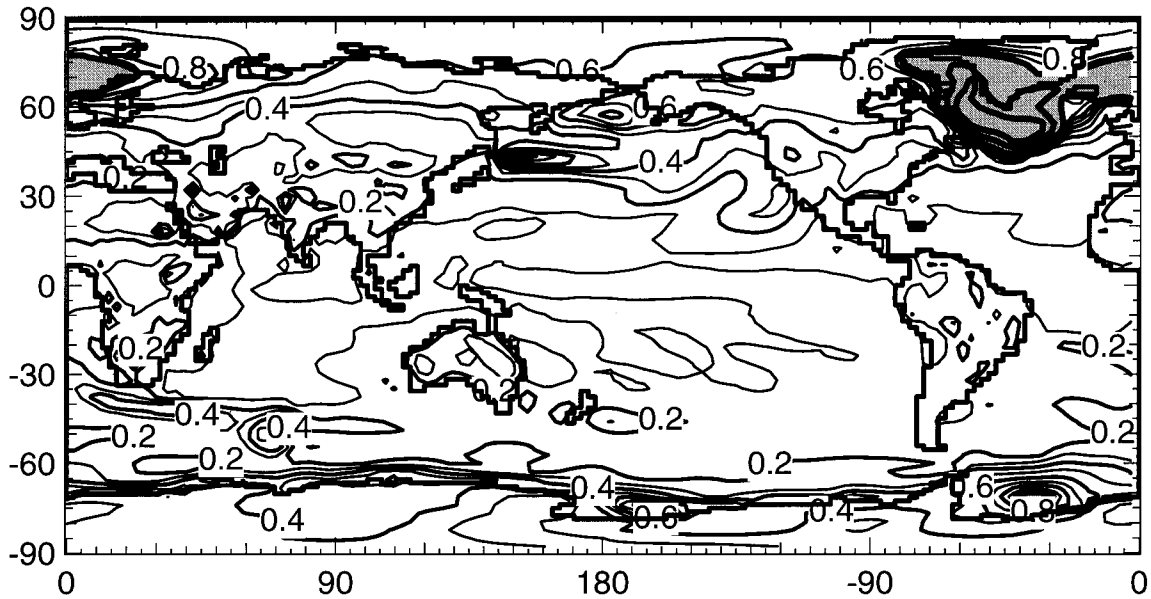
(−1.859 to 29.631 by 2) °C
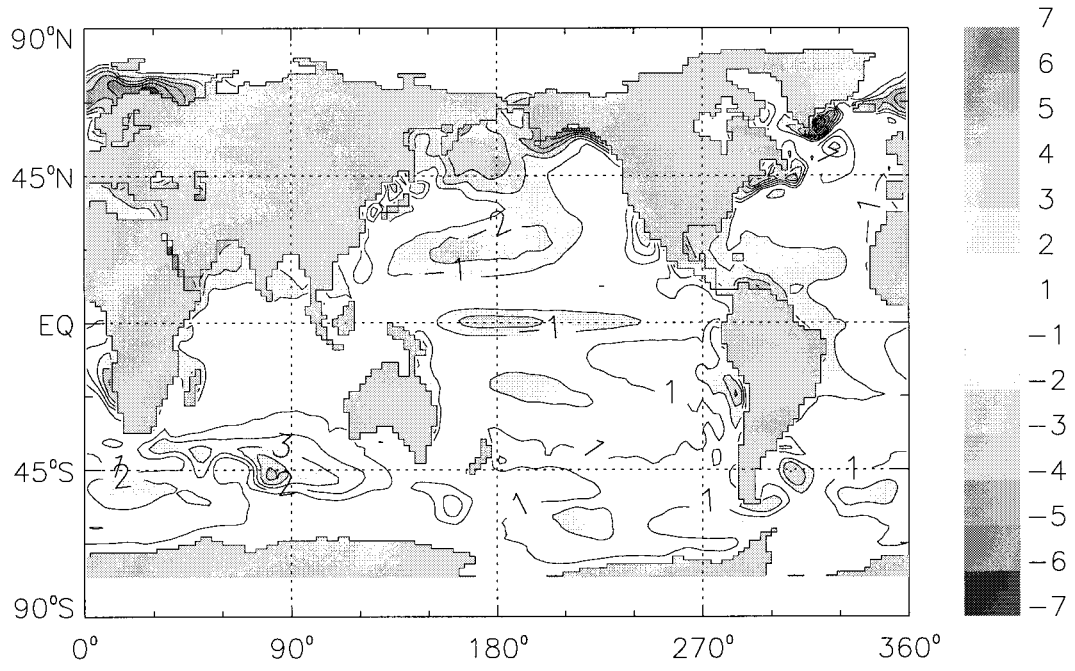
(−7.670 to   6.127 by 1) °C

FIG. 9. (a) Simulated sea surface temperatures averaged over years 91–100. The contour interval is 2°C. (b) Difference between the simulated SST and climatological temperatures for 1950–79. The contour interval is 1°C and magnitudes less than 1°C are unshaded.

Annual Mean Surface Temperature

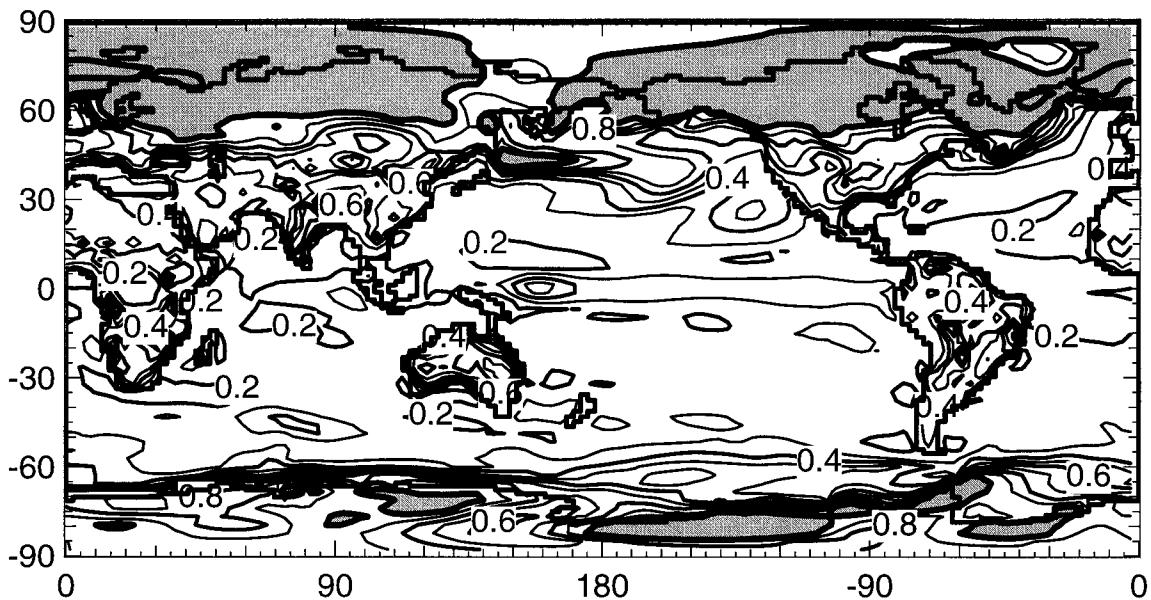### Interdecadal Variability (K)

Subdecadal Variability (K)

FIG. 10. (a) Interdecadal variability (standard deviation) and (b) subdecadal variability of the surface temperature for years 10–299 of the coupled simulation. The contour interval is 0.1 K for values <1 K. Values >1 K are shaded and contoured at 1 K.

real world. The average ice thickness is about right over much of the Arctic, but locally there are regions with ice that is much too thick [see Weatherly et al. (1998) in this issue]. The interannual variability of sea-ice thickness is realistically simulated, not underestimated as in some climate models (see Battisti et al. 1997).

Maps of the ice concentrations for March and September of years 90–99 are shown in Fig. 13. These are the months at which the maximum and minimum ice areas usually occur. In northern winter, there is a considerable amount of thin, relatively noncompact ice in the North Pacific, which accounts for most of the excess ice area. During

Ice Area (10^{13} m^2)
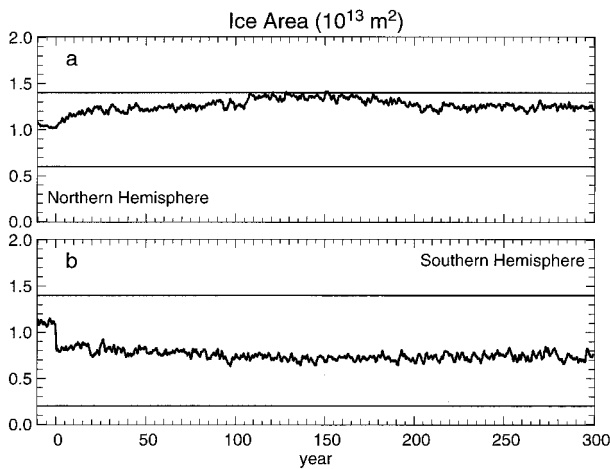
Ice volume (10^{13} m^3)

FIG. 11. (a) Northern Hemisphere ice area, and (b) Southern Hemisphere ice area during the last 10 yr of the spinup procedure and the 300-yr fully coupled run. Solid lines are the 12-month running mean from the model and observational estimates of the maximum and minimum areas. The shading indicates the annual range of the model monthly mean values.

FIG. 12. The same as Fig. 11 but for sea-ice volumes.

the years 110–190, the winter ice line in the North Atlantic extends further south, frequently reaching Newfoundland, and is responsible for the decadal variability in surface temperature noted above. Interestingly, this period also shows a decrease in northward heat transport in the Atlantic Ocean (see Capotondi and Holland 1998, manuscript submitted to *J. Climate*).

The maximum ice areas in the Southern Hemisphere drop to the observed level (Gloersen et al. 1992) almost immediately in the coupled simulation, giving an annual cycle of ice area that matches observations and remains stable throughout. The total volume also matches the estimated volume very closely, indicating that the simulated ice is about the correct thickness. The ice retreats back to the Antarctic coast in summer, while extensive regions of relatively thin, noncompact ice are found in winter, in agreement with observations. Much more detailed analysis of the sea-ice distributions can be found in Weatherly et al. (1998) and Bryan (1998) in this issue.

The net fluxes of heat and freshwater from the atmosphere into the surface are shown in Fig. 14. They are discussed in much greater detail in Doney et al. (1998) in this issue. Generally, the net fluxes of heat are reasonable, with negligible net flux into land surfaces, relatively large net heat flux into the tropical Pacific Ocean, and large fluxes out of oceans in the western parts of the Northern Hemisphere oceans. However, when individual components of the heat flux are examined, significant differences are found compared to observational analyses. For example, Kiehl (1998) in this issue shows that the net flux into the warm pool (10°S–10°N, 140°–170°E) is 25 W m^{-2} in CSM-1 compared to 13 W m^{-2} calculated from TOGA COARE observations. However, the latent heat flux is 145 W
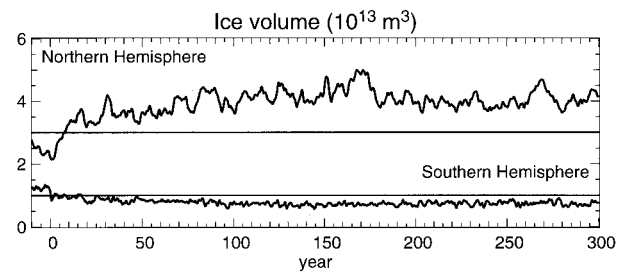
m^{-2} in CSM-1 compared to 110 W m^{-2} from the same observations.

The globally integrated surface heat flux is about 0.5 W m^{-2} into the atmosphere, whereas the top of atmosphere imbalance is less than 0.1 W m^{-2}. The remaining 0.4 W m^{-2} is lost within the atmospheric model in two ways. First, the numerical approximations conserve energy to about 0.2 W m^{-2}, partly due to the time truncation error, the intrinsically nonconservative nature of the spectral method, and the effect of water vapor on the specific heat not being consistently represented throughout CCM3. Second, there is an inconsistency in the latent heats between the CCM3 and the surface models over snow and ice. CCM3 uses only a constant latent heat of vaporization when condensing water vapor within the atmosphere. The surface models use the same constant but also include the latent heat of fusion when sublimating water vapor from snow and ice surfaces. Therefore, the energy extracted from the surface during sublimation is larger than the energy that is eventually recovered when the water vapor condenses within the atmosphere, resulting in a globally averaged net loss of 0.2 W m^{-2}. While some of these inconsistencies will be addressed in future versions of the CCM, there is little point in attempting to eliminate problems that are no larger than the truncation error in the numerical algorithms.

Problems with the freshwater flux are more obvious than those in the heat flux, reflecting significant changes in the precipitation distribution between the uncoupled CCM3 and CSM-1 simulations discussed in Boville and Hurrell (1998) in this issue. The coupled model forms a very strong double intertropical convergence zone in the Pacific Ocean, particularly in southern summer, with suppressed convection over the cold water along the equator. This feature of the precipitation can be seen in the large fluxes of freshwater into the tropical Pacific Ocean on either side of the equator with net flux into the atmosphere over the equator. The net fluxes of water into the continents can also be seen in Fig. 14, this is the term that results in runoff into the oceans and is treated crudely in CSM-1, as discussed above. There is too much precipitation over the Tibetan Plateau and the Andes, resulting in large net water fluxes there. This results from a common tendency in atmospheric GCMs to lock the precipitation over high topography. Other

Sea Ice Concentration
Years 90 - 99

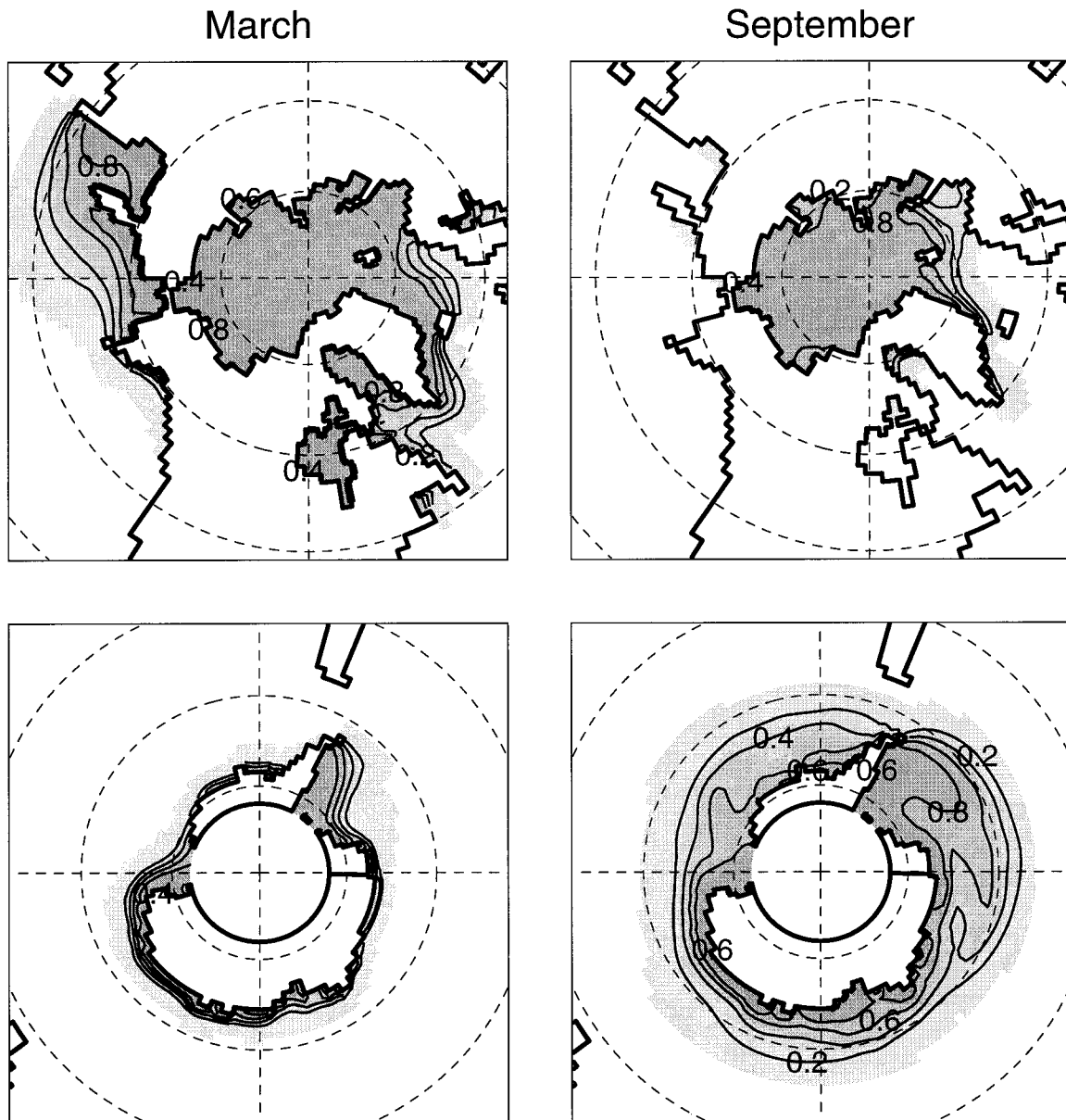### March   September

FIG. 13. Sea-ice concentrations (contour interval 0.2) in the Northern and Southern Hemispheres averaged over March and September of years 90–99. Areas with sea ice present at any time are shaded.

than the shift in tropical precipitation, the atmospheric circulation changes remarkably little in CSM-1 compared to CCM3. These changes are discussed in Boville and Hurrell (1998) and Raphael (1998), where the quasi-stationary waves in the Southern Hemisphere are examined in detail and the impact of the predicted SST and sea-ice distributions is shown.

The northward ocean heat transport from the uncoupled NCOM simulation 2 forced by NCEP atmospheric state variables is quite similar to the implied ocean heat transport from CCM3 driven by climatological SSTs. Figure 15a shows that the main difference is in low latitudes of the Northern Hemisphere. This similarity is a major reason for the lack of drift of the coupled model following a relatively short spinup experiment and for the relatively small errors in the simulated SSTs (shown in Fig. 9). The ocean and sea-ice spinup experiment driven by CCM3 fluxes gives an ocean heat transport that lies generally between the ocean heat transports in the uncoupled experiments and
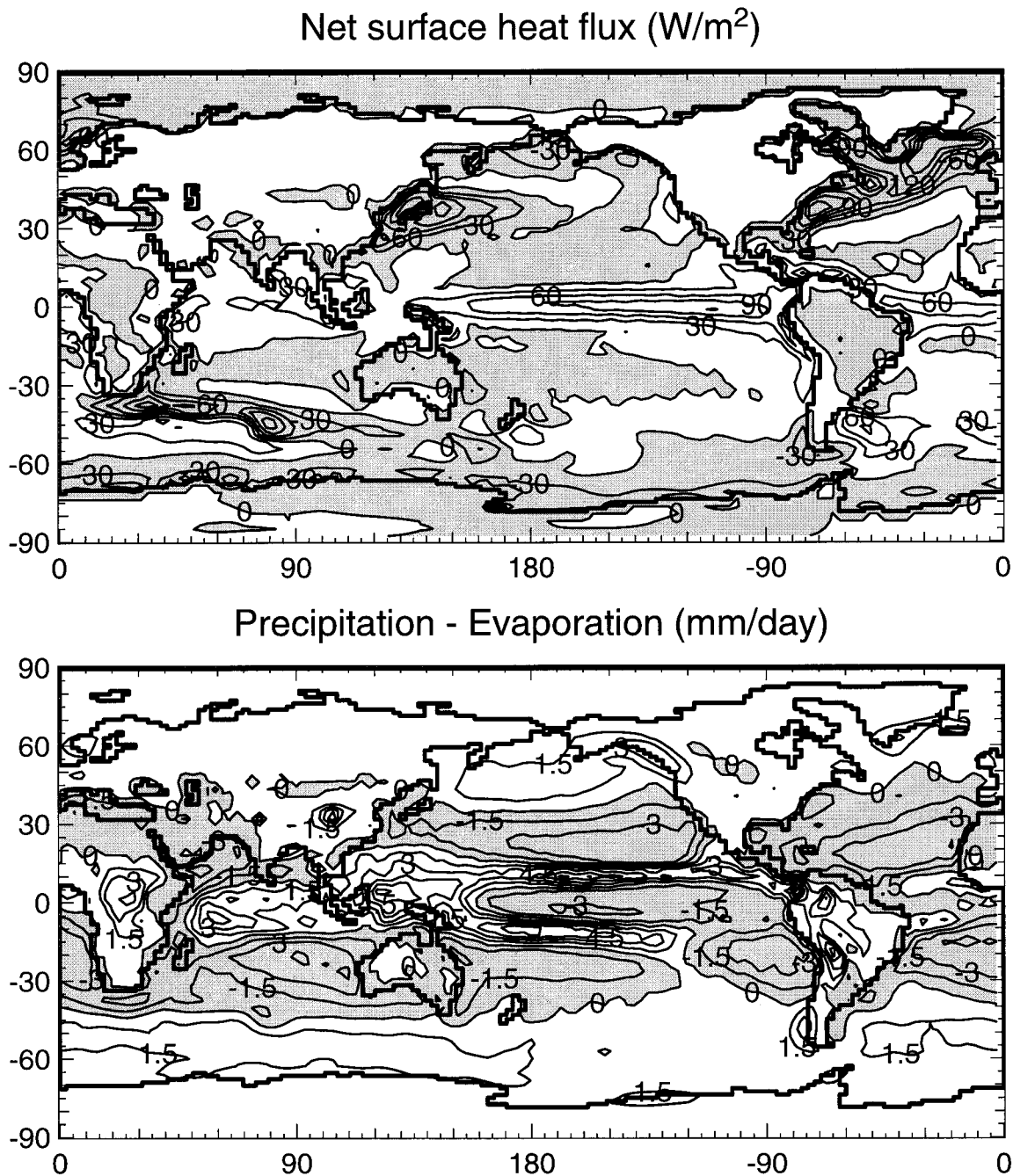
Net surface heat flux (W/m^2)

Precipitation - Evaporation (mm/day)

FIG. 14. (a) Net surface heat flux (contoured at 30 W m^{-2}) and (b) precipitation minus evaporation (contoured at 1.5 mm day^{-1}) averaged over years 90–99 of the coupled run. Negative values are shaded.

is almost identical to the ocean heat transport in the coupled simulation (see Fig. 15a). The simulated ocean heat transports are very similar to transports calculated from NCEP reanalysis data, which differ significantly from previous estimates in the Southern Hemisphere, Trenberth (1997, personal communication). In CSM-1 the ocean heat transport from the ocean model and that implied from the atmospheric model are the same, which is not generally true of flux-corrected models, since the

correction to the surface heat flux constitutes an implied ocean heat transport.

In addition to the successes described above, the 300-yr coupled run also has some very obvious deficiencies compared to the earth's climate. Several of these will be briefly mentioned here along with the reference if the problem is addressed in more detail in another paper in this issue. There are several deficiencies in the tropical Pacific region. There is a double intertropical con-
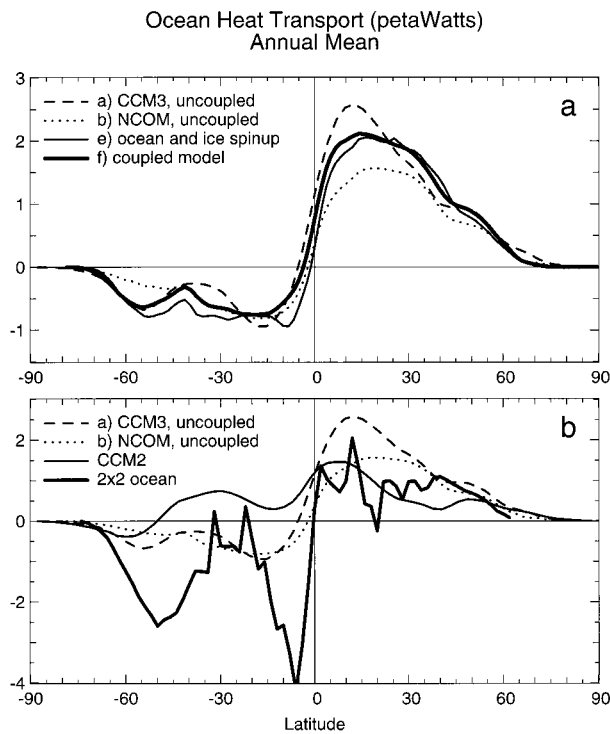
FIG. 15. Annual mean northward heat transports in PW from ocean models and the implied ocean transport from atmospheric models. (a) CCM3 uncoupled, NCOM ×2 uncoupled, ocean and ice spinup, and fully coupled model. (b) CCM3 uncoupled, NCOM ×2 ocean uncoupled, CCM2 uncoupled, and the 2° ocean model curve from Fig. 10 of Covey (1995).
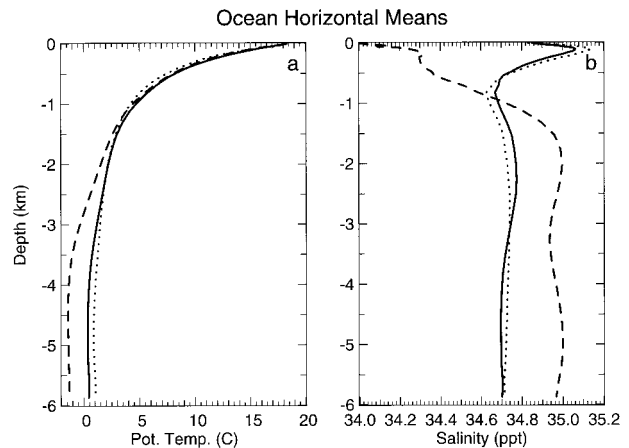

FIG. 16. (a) Area-averaged potential temperature and (b) area-averaged salinity plotted against depth. The curves are the Levitus climatology (dotted), uncoupled NCOM equilibrium (solid), and the average of years 250–300 of the fully coupled run (dashed).

vergence zone that is more symmetric about the equator than reality and the cold tongue is too strong in the equatorial Pacific Ocean. There is a deficiency in the amount of marine stratus clouds in the Tropics with consequently higher than observed SSTs in these regions. The heat budget of the Pacific warm pool is inconsistent with observations [see Kiehl (1998) and Meehl and Arblaster (1998) in this issue].

Several aspects of the ocean circulation are unrealistic. The Antarctic Circumpolar Current in the model is statistically steady, but its mean value through Drake Passage is about 240 Sv (Sv ≡ 10^6 m^3 s^{-1}), which is double the observed value. This is tied in with the meridional overturning circulation on the Antarctic shelf, which is much stronger than in reality or the ocean-alone integration 2 (see Bryan 1998). The North Atlantic overturning in the coupled run varies between 25 and 30 Sv, which is stronger than the ocean-alone solution of about 20 Sv and the observed estimate of about 18 Sv (see Capotondi and Holland 1998, manuscript submitted to *J. Climate*). The North Atlantic overturning has quite strong variability, but only a small trend in the fully coupled run. However, the wind-driven ocean circulation does not change much between the spinup and the fully coupled runs, because the atmospheric

circulation is quite similar [see Boville and Hurrell (1998) and Danabasoglu (1998) in this issue].

Figures 11 and 13 show that there is too much sea ice in the Arctic in the coupled run. The ice is too extensive in that it reaches too far south primarily in the North Pacific but also in the North Atlantic Ocean, as mentioned above. The thickest ice is thicker than observed and occurs in the Arctic Ocean near the Siberian coast and Bering Strait, whereas, in reality, the thickest Arctic ice is adjacent to northern Canada (see Weatherly et al. 1998 in this issue). The problems in the Arctic Ocean and sea-ice distributions have been exacerbated by two poor facets of the 300-yr coupled run. The first is the lack of a river runoff model, so that the significant freshwater source from rivers into the Arctic Ocean is missing. The second is the increase in the volume of Arctic sea ice during the coupled run, which resulted in a significant increase of the Arctic Ocean surface salinity.

Although there is virtually no trend in the ocean model SSTs, there are quite strong trends in the deeper temperatures and in salinity at all depths of the ocean. Figure 5 shows the area-averaged potential temperature and salinity at level 38 in the ocean model, which is about 4 km deep, during the coupled run. The potential temperature does not change substantially during the run but is increasing at the end, whereas it reduced substantially during the spinup phase. In contrast, the salinity shows a monotonic increase during the coupled run, which continues the substantial increase during the spinup phase. At the end of the coupled run, the average salinity at 4 km is nearly 35 ppt, which is much too saline. Figure 16 shows the area-averaged potential temperature and salinity as a function of depth averaged over years 250–300 of the coupled run, as well as those from the ocean-alone equilibrium run 2 and the observations of Levitus (1982). The ocean below 2 km is

considerably colder than reality and is only slightly warmer than the sea-ice freezing point of $-1.8°C$. The ocean salinity profile has been changed drastically from the ocean alone equilibrium run 2, which is quite close to the observations. The upper ocean is much too fresh and the ocean below 1 km much too saline compared to reality. The drift in salinity is discussed more fully in Bryan (1998) in this issue and would have continued if the coupled model had been run further. Sooner or later, the ocean circulation would have changed substantially away from the present climate. This is the main reason why the coupled run was stopped after 300 yr.

5. Discussion and conclusions

The NCAR Climate System Model version one has been run in fully coupled mode for 300 yr. There is no correction in the heat fluxes transferred between the atmosphere and the ocean, sea ice, and land. Water fluxes are adjusted only to ensure global conservation of water in the absence of a river runoff model. The surface temperatures have virtually no trend in the integration, but they have interesting variability of a reasonable magnitude on all timescales. This is the major success of this coupled integration. However, there are significant drifts in the deep ocean, which is the model component with the longest timescales. We now try to address why the CSM-1 has achieved this success. We believe there is a two-part answer: the first is the state-of-the-art component models, and the second is the spinup procedure used.

The implied ocean heat transport from the uncoupled integration 1 of CCM3 is shown in Fig. 15b, along with the equivalent curve from the previous version of the atmospheric model CCM2. The curves are quite different, and CCM2 implies a substantial equatorward transport in the Southern Hemisphere north of 50°S, consistent with many other atmospheric GCMs as shown by Gleckler et al. (1995). This is inconsistent with all ocean model results and observations. Hack (1998) in this issue shows that the major factor contributing to the CCM3 curve is the new penetrative convection parameterization, which alters the atmospheric humidity, resulting in changes in the surface latent heat fluxes, the cloud distribution, and the radiation budget.

The previous generation of coarse resolution global ocean models did not contain the mesoscale eddy parameterization of Gent and McWilliams (1990) and used surface boundary conditions of strong restoring to observations. Ocean heat transports from these models are shown in Fig. 10 of Covey (1995), and the curve from that figure for a resolution of 2° × 2° is reproduced in Fig. 15b, along with the equivalent curve from NCOM. NCOM has an increased transport in the Northern Hemisphere and a considerably reduced transport in the Southern Hemisphere compared to the Covey (1995) curve. Figure 2 of Large et al. (1997) shows that most

of the improvement in the heat transport comes from the effect of the mesoscale eddy parameterization, while the improved method of forcing the model greatly improves the salinity distribution and freshwater transport in NCOM. We believe that compatible heat transports in the component models are a prerequisite for a stable and accurate surface temperature in a coupled integration. We infer that this would not have occurred if CCM2 had been coupled to a previous generation, coarse resolution global ocean model. Further, improving only one of the components would still not result in a stable and accurate simulation of surface temperature.

The second important precursor to producing a coupled run with stable surface temperatures was the spinup procedure, which produced compatible initial conditions in the component models. Even so, improvements could have been made to the spinup procedure. The ice-albedo feedback had to be turned off in run 3 described above. Perhaps this would not have been necessary if the ocean and sea-ice models had been spun up together using observed forcing, instead of just the ocean model, as described in 2. Doing this would also have shown earlier problems with the solution in 3 when the ocean and ice models were forced with CCM3 data. As mentioned in section 3, the sea-ice areas diagnosed from the STR SST dataset are somewhat larger than observations. This method of diagnosing sea-ice extent is used in both the CCM3 and NCOM alone spinups described in 1 and 2. These spinups would have been better with a more realistic sea-ice diagnosis, and so would the ocean and ice spinup described in 3 above. Second, the equilibrium ice volume in the coupled run in the Arctic was more than double that in the initial condition. This ice formation rejected a large amount of salt into the Arctic Ocean, which combined with the lack of river discharge there to eliminate the Arctic surface halocline very quickly [see Bryan (1998) in this issue]. Perhaps it would have been better to switch off this component of the ice–ocean interaction in the coupled run until the sea-ice volume had come much nearer to its equilibrium value.

How long should the ocean and sea-ice spinup integrations 3 and 4 have been run? The decision to stop after 50 yr, corresponding to 500 yr in the deep ocean, was made because the trends in the deep ocean temperatures and surface salinity had reduced considerably. It also meant that the deep ocean trends did not have time to take the ocean simulation too far from the quite realistic state obtained in run 2. Gent et al. (1998) documents how trends in the ocean salinity distribution can continue for many hundreds of years, because there is no local feedback of surface salinity on the surface heat and freshwater fluxes. So the spinup solution would have deteriorated in this respect if it had been integrated longer: instead the trends continued in the fully coupled run (see Fig. 5). We assume that these drifts in the ocean model would eventually lead to a significantly different

ocean circulation, not like the present climate, if the coupled run had been integrated longer, although it is not obvious when this would occur. It is also worth pointing out that it does not make sense to run the ocean and ice spinup forced by CCM3 data out for the very long time it takes the ocean to come into equilibrium as the first step in reaching a coupled model equilibrium solution. The reason is that the atmospheric circulation rapidly changes when it is coupled, so a short coupled run should be made to obtain a new CCM3 dataset. Then the ocean and ice models should be run further forced by the new dataset. A succession of ocean and ice alone and fully coupled integrations would be the quickest way to reach a coupled equilibrium solution.

The simulation with the NCAR CSM version 1 needs many improvements. It is obvious that a river runoff model is needed, which could be used in all stages of the spinup procedure. This will require changes to both the CSM ocean and land models. Kiehl (1998) in this issue documents problems with the CCM3 heat budget in the Pacific warm pool and suggests changes are needed to the absorption of solar insolation in CCM3. Bryan (1998) in this issue documents problems with the strength of the overturning on the Antarctic shelf and the Antarctic Circumpolar Current and suggests changes are needed to the sea-ice model rheology. We believe these will be necessary steps to eliminate deep ocean drifts and obtain stable solutions on millennial time-scales without flux corrections. We also believe this is an even more difficult challenge than obtaining stable solutions of the upper-ocean temperature and atmosphere on centennial timescales without flux corrections, which has been achieved so far. This challenge will be addressed with future versions of the NCAR Climate System Model.

REFERENCES

Battisti, D. S., C. M. Bitz, and R. E. Moritz, 1997: Do general circulation models underestimate the natural variability in the Arctic climate? *J. Climate,* **10,** 1909–1920.

Bonan, G., 1998: The land surface climatology of the NCAR Land Surface Model (LSM 1.0) coupled to the NCAR Community Climate Model (CCM3). *J. Climate,* **11,** 1307–1326.

Boville, B. A., and J. Hurrell, 1998: A comparison of the atmospheric circulations in CCM3 and CSM1. *J. Climate,* **11,** 1327–1341.

Briegleb, B. P., and D. H. Bromwich, 1998a: Polar radiation budgets of the NCAR CCM3. *J. Climate,* **11,** 1246–1269.

——, and ——, 1998b: Polar climate simulation of the NCAR CCM3. *J. Climate,* **11,** 1270–1286.

Bryan, F. O., 1998: Climate drift in a multi-century integration of the NCAR Climate System Model. *J. Climate,* **11,** 1455–1471.

——, B. G. Kauffman, W. G. Large, and P. R. Gent, 1996: The NCAR CSM flux coupler. NCAR Tech. Note 424, 50 pp. [Available from NCAR, Boulder, CO 80307.]

Bryan, K., 1984: Accelerating the convergence to equilibrium of ocean-climate models. *J. Phys. Oceanogr.,* **14,** 666–673.

Covey, C., 1995: Global ocean circulation and equator-pole heat transport as a function of ocean GCM resolution. *Climate Dyn.,* **11,** 425–437.

Danabasoglu, G., 1998: On the wind-driven circulation of the uncoupled and coupled NCAR Climate System Ocean Model. *J. Climate,* **11,** 1442–1454.

——, J. C. McWilliams, and W. G. Large, 1996: Approach to equilibrium in accelerated global oceanic models. *J. Climate,* **9,** 1092–1110.

Doney, S. C., W. G. Large, and F. O. Bryan, 1998: Surface ocean fluxes and water-mass transformation rates in the coupled NCAR Climate System Model. *J. Climate,* **11,** 1420–1441.

Flato, G. M., and W. D. Hibler, 1990: On a simple sea ice dynamics model for climate studies. *Advances in Geophysics,* Vol. 14, Academic Press, 72–77.

——, and ——, 1992: Modeling ice pack as a cavitating fluid. *J. Phys. Oceanogr.,* **22,** 626–651.

Gates, W. L., and Coauthors, 1996: Climate models—Evaluation. *Climate Change 1995: The Science of Climate Change,* J. T. Houghton, L. G. Meira Filho, B. A. Callander, N. Harris, A. Kattenberg, and K. Maskell, Eds., Cambridge University Press, 229–284.

Gent, P. R., and M. A. Cane, 1989: A reduced gravity, primitive equation model of the upper equatorial ocean. *J. Comput. Phys.,* **81,** 444–480.

——, and J. C. McWilliams, 1990: Isopycnal mixing in ocean circulation models. *J. Phys. Oceanogr.,* **20,** 150–155.

——, J. Willebrand, T. J. McDougall, and J. C. McWilliams, 1995: Parameterizing eddy-induced tracer transports in ocean circulation models. *J. Phys. Oceanogr.,* **25,** 463–474.

——, F. O. Bryan, G. Danabasoglu, S. C. Doney, W. R. Holland, W. G. Large, and J. C. McWilliams, 1998: The NCAR Climate System Model global ocean component. *J. Climate,* **11,** 1287–1306.

Gleckler, P. J., and Coauthors, 1995: Cloud-radiative effects on implied oceanic energy transports as simulated by atmospheric general circulation models. *Geophys. Res. Lett.,* **22,** 791–794.

Gloersen, P., W. J. Campbell, D. J. Cavalieri, J. C. Comiso, C. L. Parkinson, and H. J. Zwally, 1992: Arctic and Antarctic Sea Ice, 1978–1987: Satellite passive-microwave observations and analysis. U.S. Natl. Aeron. Space Admin. Special Publ. NASA SP-511, 290 pp.

Hack, J. J., 1994: Parameterization of moist convection in the NCAR Community Climate Model (CCM2). *J. Geophys. Res.,* **99,** 5551–5568.

——, 1998: An analysis of the improvement in implied meridional ocean energy transport as simulated by the NCAR CCM3. *J. Climate,* **11,** 1237–1244.

——, J. T. Kiehl, and J. Hurrell, 1998: The hydrologic and thermodynamic characteristics of the NCAR CCM3. *J. Climate,* **11,** 1179–1206.

Holland, W. R., J. H. C. Chow, and F. O. Bryan, 1998: Application of a third-order upwind scheme in the NCAR ocean model. *J. Climate,* **11,** 1487–1493.

Holtslag, A. A. M., and B. A. Boville, 1993: Local versus non-local boundary layer diffusion in a global climate model. *J. Climate,* **6,** 1825–1842.

Hurrell, J., J. J. Hack, B. A. Boville, D. Williamson, and J. T. Kiehl,

1998: The dynamical simulation of the NCAR Community Climate Model version 3 (CCM3). *J. Climate,* **11,** 1207–1236.

Kattenberg, A., and Coauthors, 1996: Climate models—Projections of future climate. *Climate Change 1995: The Science of Climate Change,* J. T. Houghton, L. G. Meira Filho, B. A. Callander, N. Harris, A. Kattenberg, and K. Maskell, Eds., Cambridge University Press, 285–357.

Kiehl, J. T., 1998: Simulation of the tropical Pacific warm pool with the NCAR Climate System Model. *J. Climate,* **11,** 1342–1355.

——, J. J. Hack, G. Bonan, B. A. Boville, D. Williamson, and P. Rasch, 1998a: The National Center for Atmospheric Research Community Climate Model: CCM3. *J. Climate,* **11,** 1131–1149.

——, ——, and J. Hurrell, 1998b: The energy budget of the NCAR Community Climate Model: CCM3. *J. Climate,* **11,** 1151–1178.

Large, W. G., J. C. McWilliams, and S. C. Doney, 1994: Oceanic vertical mixing: A review and a model with a nonlocal boundary layer parameterization. *Rev. Geophys.,* **32,** 363–403.

——, G. Danabasoglu, S. C. Doney, and J. C. McWilliams, 1997: Sensitivity to surface forcing and boundary layer mixing in the NCAR CSM ocean model: Annual-mean climatology. *J. Phys. Oceanogr.,* **27,** 2418–2447.

Levitus, S., 1982: *Climatological Atlas of the World Ocean.* NOAA Prof. Paper 13, U.S. Govt. Printing Office, 173 pp. [Available from GFDL, P.O. Box 308, Princeton, NJ 08540.]

Meehl, G. A., and J. Arblaster, 1998: The Asian–Australian monsoon and El Niño–Southern Oscillation in the NCAR Climate System Model. *J. Climate,* **11,** 1356–1385.

——, G. J. Boer, C. Covey, M. Latif, and R. Stouffer, 1997: Analyzing and intercomparing global coupled atmosphere–ocean-sea ice climate models. *Eos, Trans. Amer. Geophys. Union,* **78,** 445–451.

Raphael, M., 1998: Quasi-stationary waves in the Southern Hemisphere: An examination of their simulation by the NCAR Climate System Model with and without an interactive ocean. *J. Climate,* **11,** 1405–1418.

Reynolds, R. W., and T. M. Smith, 1994: Improved global sea surface temperature analysis using optimum interpolation. *J. Climate,* **7,** 929–948.

Saravanan, R., 1998: Atmospheric low-frequency variability and its relationship to midlatitude SST variability: Studies using the NCAR Climate System Model. *J. Climate,* **11,** 1386–1404.

Semtner, A. J., 1976: A model for the thermodynamic growth of sea ice in numerical investigations of climate. *J. Phys. Oceanogr.,* **6,** 379–389.

Shea, D. J., K. E. Trenberth, and R. W. Reynolds, 1990: A global monthly sea surface temperature climatology. NCAR Tech. Note NCAR/TN-345, 167 pp.

Washington, W. M., and G. A. Meehl, 1996: High latitude climate change in a global coupled ocean-atmosphere-sea ice model with increased atmospheric CO_2. *J. Geophys. Res.,* **101,** 12 795–12 801.

Weatherly, J., B. Briegleb, W. G. Large, and J. Maslanik, 1998: Sea ice and polar climate in the NCAR CSM. *J. Climate,* **11,** 1472–1486.

Zhang, G. J., and N. A. McFarlane, 1995: Sensitivity of climate simulations to the parameterization of cumulus convection in the Canadian Climate Centre general circulation model. *Atmos.–Ocean.,* **33,** 407–446.